Relative phase locking of pulses in a passively mode-locked fiber laser

Philippe Grelu, Franck Belhache, and François Gutty

Laboratoire de Physique de l'Université de Bourgogne, Unite Mixte de Recherche 5027, B.P. 47870, Dijon F-21078, France

Jose M. Soto-Crespo

Instituto de Optica, Consejo Superior de Investigaciones Científicas, Serrano 121, Madrid 28006, Spain

Received May 10, 2002; revised manuscript received November 21, 2002

In a passively mode-locked fiber ring laser, we report the experimental observation of relative phase locking of pulses in a wide variety of cases. Relative phase locking is observed in bunches of N pulses separated by more than 20 pulse widths as well as in close pulse pairs. In the latter case, the phase relationship between the two pulses is measured to be $\pm\pi/2$, which is related to theoretical predictions formerly obtained from a Ginzburg–Landau distributed model. We have developed a simplified numerical model adapted to our laser, which keeps its essential features while significantly reducing the number of free parameters. The agreement with the experiment is excellent. © 2003 Optical Society of America

OCIS codes: 060.5530, 140.3510, 190.4410, 230.2090.

1. INTRODUCTION

Multiple pulsing has been observed in different kinds of passively mode-locked laser configuration. In fiber lasers, this behavior was reported in the early experiments and was related to solitonic pulse shaping in the anomalous dispersion regime, which tends to quantize the pulse energy.[1–4] It was then noted that, depending on the mode-locking conditions, the pulses could either space themselves equally along the cavity, group into a tight bunch, or be more or less randomly distributed.[1] Multiple pulsing was also reported within the context of ultrashort pulse generation with Ti:sapphire or Cr:forsterite lasers.[5–8] To understand multipulse operation with passive mode locking, two phenomena have to be addressed: pulse splitting, which is the way additional pulses can appear in the cavity, and pulse-to-pulse interaction, which could eventually lead to the stabilization of pulse spacing. Pulse splitting arises naturally with an increase of the pulse energy within the framework of higher-order soliton formation. However, the temporal profile of a high-order soliton is not stationary and undergoes periodic evolution along the space coordinate. In addition, pulse splitting can be favored when the pulse travels through separate sections having different properties during its round trip in the cavity.[6] This is the case for Ti:sapphire lasers for which anomalous dispersion and self-phase modulation arise separately, or for fiber lasers that comprise separate regions of high gain and losses. The periodic perturbations scatter the main pulse energy into dispersive waves.[9] For some spectral components, resonant scattering occurs, which is responsible for large radiative losses.[10] Turning a single-pulse operation into a multipulse operation while keeping approximately the same amount of total intracavity energy induces lower radiative losses and stabilizes the mode-locking operation.[11,12] However, to lead to a stabilization of multiple pulsing, higher-order effects,[13] such as gain saturation or third- and fourth-order dispersion, are to be considered in most cases. In a linear resonator cavity, the nonlinear interaction of colliding pulses in a Kerr medium was shown to be responsible for a stable two-pulse operation with a continuously tunable separation.[7] However, in the following we restrict ourselves to the study of unidirectional ring cavities. Dealing with sub-100 fs pulses, third- and fourth-order dispersion terms can play a key role in the stabilization of multiple pulsing.[8,11] For longer pulse durations, other nonlinearities could prove to have a major influence on multiple pulsing. On the theoretical side, optical systems such as fiber lasers and optical transmission lines, modeled with the complex nonlinear Ginzburg–Landau equation, which features nonlinear saturating gain and spectral filtering, were shown to support stable multisoliton solutions.[14,15] Recently we experimentally obtained two-pulse operations of a fiber ring laser, which are consistent with these theoretical predictions.[16]

With fiber lasers, harmonic mode locking, which means the equal spacing of pulses all along the cavity, attracts most of the attention in view of the development of high-repetition-rate sources for telecom applications.[17,18] However, a large timing jitter between pulses was observed, and it was thought that ultrashort pulses being separated by more than ten pulse widths would always suffer such position instability. Consequently, high-repetition-rate sources have been developed mainly within the framework of active mode locking,[19–21] although interesting alternatives have been demonstrated.[22,23] Still, in passively mode-locked fiber lasers, recent observations of bunches that consist of several pulses separated by tens of pulse widths have stressed

the high stability of the bunch structure. Rearrangement dynamics has been reported[24] as well as regular bunching with very low timing jitter.[12] A remarkable feature, which seems restricted to the field of fiber lasers, is the ability of pulses to bunch with a large range of possible separations, from a few to several hundred pulse widths. When pulses are largely separated in a bunch, electrostrictive effects that are peculiar to the optical fiber medium could play a key role to maintain the bunch structure.[18,25] A different mechanism that could have an effect on multiple pulsing is gain depletion and recovery,[26] which applies to fiber lasers and bulk lasers as well and provides a repulsive force between pulses that tends to favor harmonic mode locking. However this weak force cannot suppress pulse-to-pulse timing jitter.

In the research reported here, we show that pulses that bunch in our passively mode-locked fiber laser maintain a fixed phase relationship in a wide variety of cases. In Section 2 we describe the observation of phase-locked bunches of pulses separated from typically 20 to 50 pulse widths. The electrostrictive effect, which is not sensitive to the phase of the optical field, could not be solely responsible for such pulse locking. A coherent effect, such as a soliton–soliton type interaction, must be sought. When shorter pulse separations are obtained, soliton–soliton interactions dominate.[27] By changing the mode-locking conditions of our fiber laser, we could also maintain two interacting pulses within 4–10 pulse widths and measure their phase difference precisely, showing evidence of soliton–soliton interaction.[16] In Section 3 we detail these experimental results. Section 4 is devoted to the description of a new propagation model that was adapted to the case of fiber ring laser cavities in which passive mode locking relies on nonlinear polarization evolution. The numerical results that we have obtained show similar formation of phase-locked pulse pairs.

2. PHASE-LOCKED BUNCHES OF PULSES

The following experimental results were obtained with a stretched-pulse fiber ring laser that operates near 1530 nm.[28,29] This ring configuration, as shown in Fig. 1(a), features dispersion management and passive mode-locking through nonlinear polarization evolution.[30] It comprises in series a 1400-parts-in-10^6 erbium-doped fiber (EDF) (Er741+ from Highwave Optical Technologies, Lannion, France) and provides gain in the normal dispersion regime [$D = -40$ (ps/nm)/km], a 980/1550-nm coupler–isolator combination, and an anomalous section of standard telecom SMF-28 fiber [$D = +17$ (ps/nm)/km]. The coupler–isolator combination ensures unidirectional lasing, is polarization insensitive, and also couples pump light into an EDF from a module of wavelength-multiplexed laser diodes that emit around 980 nm (SDL, Incorporated). For the precision of mode-locking adjustments, wave plates and polarizers are kept in an open-air section.[29] Nonlinear polarization evolution that takes place along the propagation in the fibers makes transmission through polarizer P1 intensity dependent, which allows for passive mode locking to be triggered by an appropriate adjustment of the preceding wave plates. This is followed by a variable-output coupler formed by a half-wave plate and a second polarizing cube (P2). Temporal characterization of the output intensity is performed by use of a laboratory-made optical autocorrelator that uses a 1-mm-thick β-barium borate crystal in type I second-harmonic generation (SHG) and can be set in an interferometric or a noninterferometric mode.

In the main series of experiments, the path-averaged dispersion was kept to a slightly anomalous value near +3 (ps/nm)/km. We used a 1.6-m length of EDF and a 4.8-m length of SMF-28. The laser self-mode locks for a pump power of more than 35 mW. In the anomalous path-averaged dispersion regime, low-pedestal sech-profiled pulses are observed with FWHM durations from 350 to 650 fs. Figure 2 shows typical spectrum and autocorrelation functions of such working points. We note that, in the presence of dispersion management, resonant spectral sidebands are reduced.[29] When the pump power is increased to greater than 80 mW, stable bunches of identical pulses can easily be obtained. While reporting the observation of equally spaced bunches of pulses separated from 20 ps,[12] we could infer from the autocorrelation traces the very low level of timing jitter, which was remarkable for pulses separated from more than 40 pulse widths. In fact, the pulses appear to be locked in time precisely, and recording the output spectrum with a high-resolution monochromator (Jobin–Yvon HR 640) reveals a channeled-spectrum structure. Figure 3(a) presents such a typical spectrum of a pair of pulses separated from 20.8 ps, which takes a few minutes to be recorded. So, the two pulses have to be phase-locked precisely to maintain such a good contrast of the interference pattern, since any timing jitter at the femtosecond scale would reduce the fringe contrast. Another proof of the phase lock-

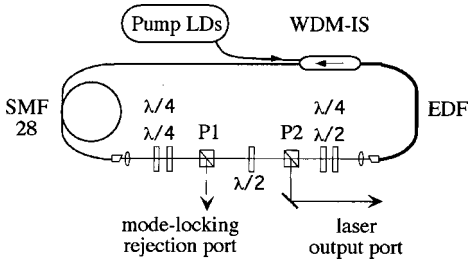

Fig. 1. Fiber ring laser experimental setup. The EDF is pumped by laser diodes (LDs) through a polarization-insensitive coupler-isolator (WDM-IS): λ/2, half-wave plate; λ/4, quarter-wave plate.

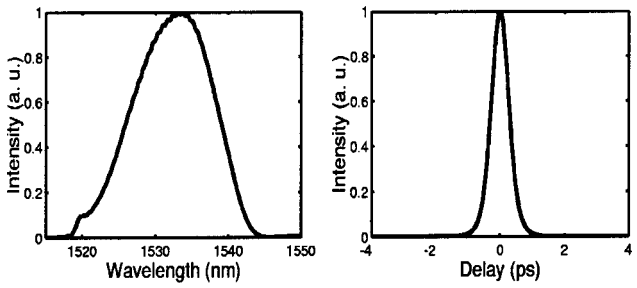

Fig. 2. Typical recorded spectrum and autocorrelation function for single-pulse operation. The spectral FWHM is 13 nm and the autocorrelation FWHM is 640 fs.

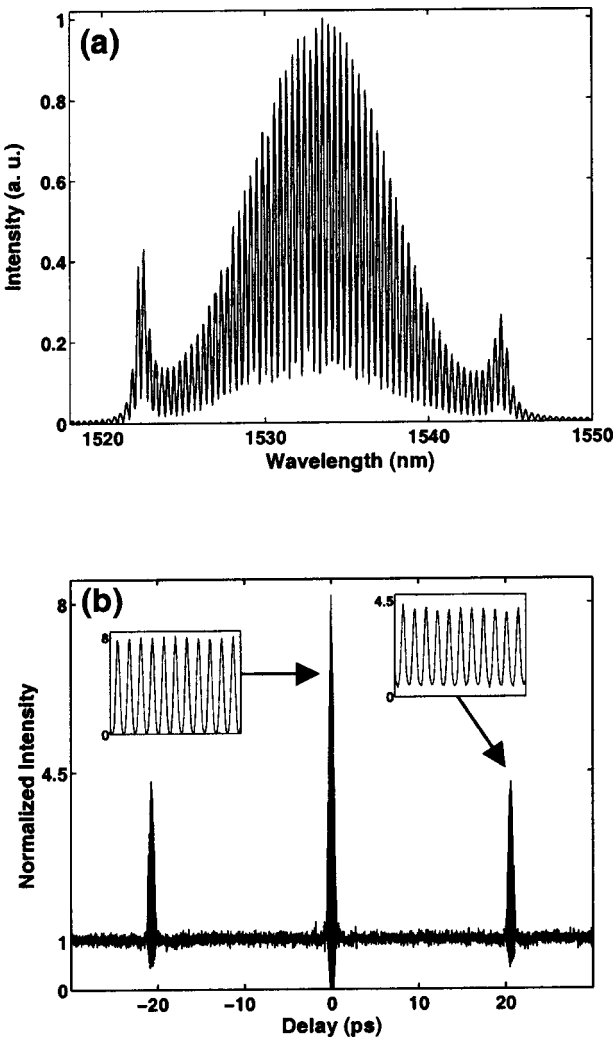

Fig. 3. (a) High-resolution spectrum of a phase-locked pulse pair. The pump power is 90 mW. The channeled-spectrum structure indicates phase locking. (b) Corresponding interferometric autocorrelation, showing two pulses separated by 20.8 ps. The insets show enlarged views of the central peak and of one lateral peak, revealing interference patterns. These patterns confirm the phase-locked state of two pulses of identical amplitude.

ing is given by the recording of the interferometric autocorrelation, as shown in Fig. 3(b). The autocorrelation traces have been normalized so that the average SHG intensity is unity where the pulses do not overlap. The side peaks correspond to the interferometric cross correlation of the two pulses. As shown in the insets, the side peaks present fringes that extend from 0.5 to 4.5, whereas for the central peak they extend from 0 to 8. To be precise, these are the expected contrasts when two pulses of the same amplitude have a fixed phase relationship. Dealing with a higher number of pulses, Gutty *et al.*[12] showed that these pulses tend to bunch with regular spacing. High-resolution spectra then have the same envelope and the same interfringe value as in Fig. 3(a), showing that all the pulses phase lock to each other. However, equal spacing does not always happen. Bunch patterns are also dependent on the history of their formation and have strong hysteresis characteristics. In Fig. 4(a) we show the spectrum of a four-pulse bunch that presents beats that reveal unequally spaced pulses, as displayed in Fig. 4(b), that is, the Fourier transform of this spectrum. The peaks in Fig. 4(b) exactly coincide with the peaks of the interferometric autocorrelation shown in Fig. 4(c). Moreover, all the peaks in Fig. 4(c) have an interference pattern structure. In our laser setup, the time separation is thus not fixed *a priori* by a linear mechanism such as intracavity birefringence. To gain more insight, we placed a 10/90-output coupler in another part of the cav-

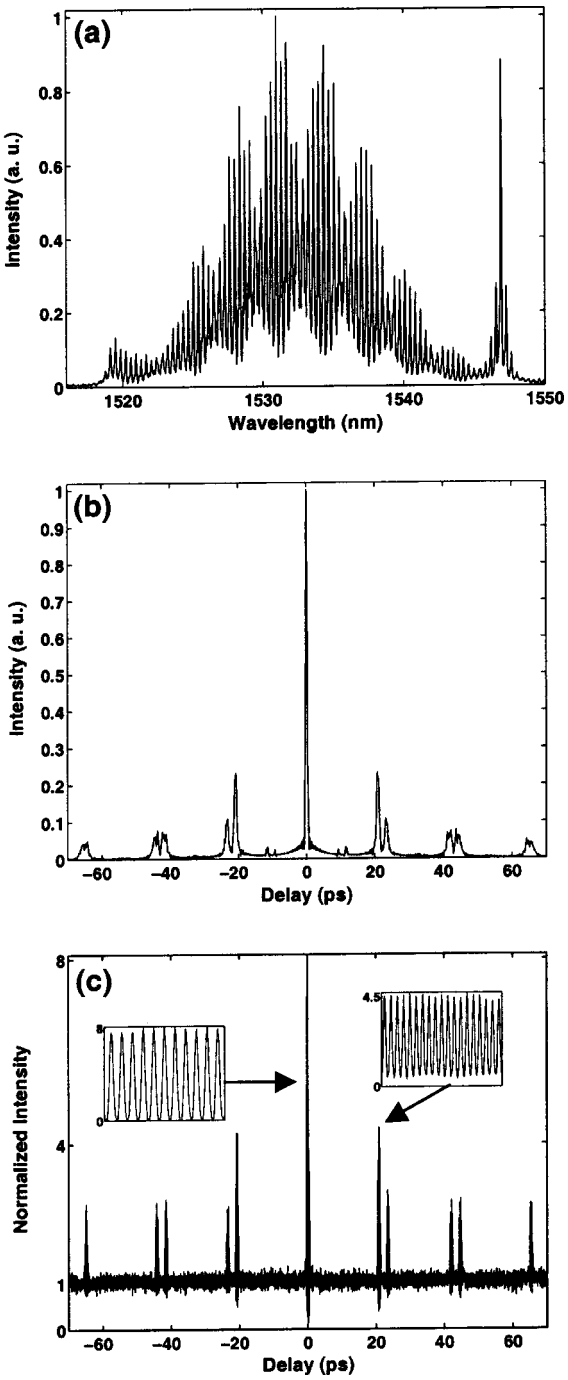

Fig. 4. (a) High-resolution spectrum of a four-pulse bunch. (b) Fourier transform of the preceding spectrum, revealing unequal separations between pulses. (c) The preceding separations (20.8 and 23.5 ps) are confirmed by this interferometric autocorrelation. Moreover, all the peaks present fringes of interference, showing phase locking between all the pulses.

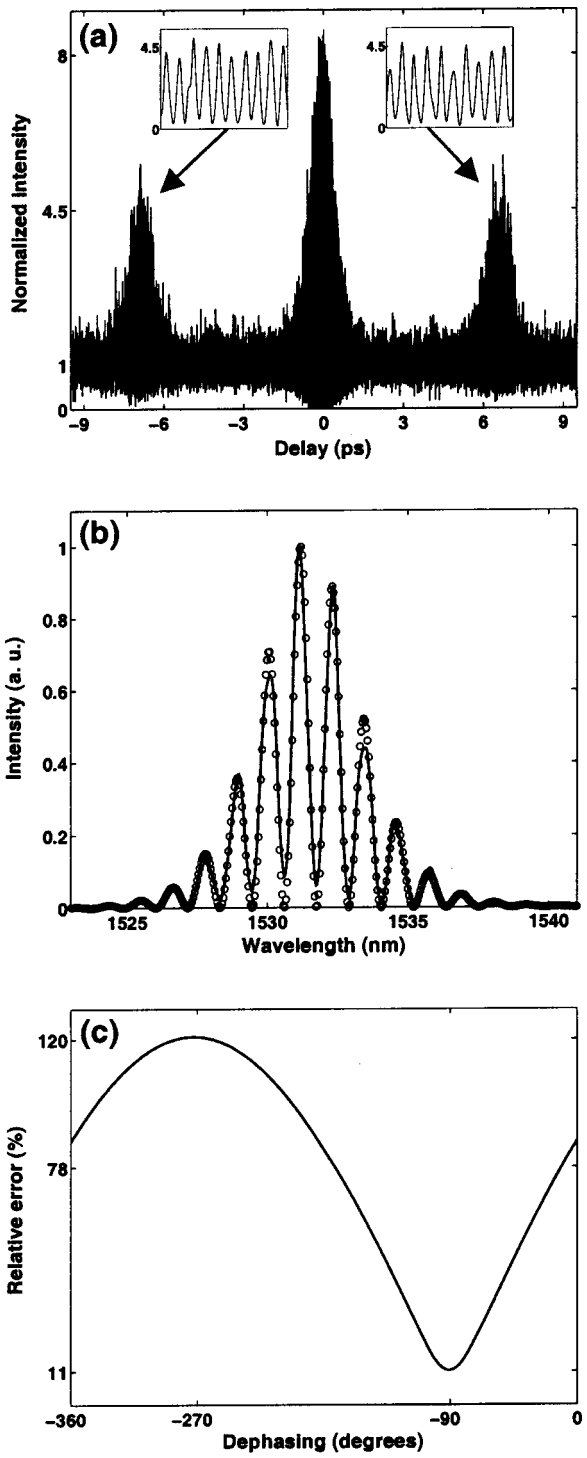

Fig. 5. (a) Interferometric autocorrelation of a pulse pair with a 6.8-ps separation. Pulse-duration measurement yields 610 fs FWHM. The insets show enlarged views of the lateral peaks that feature fringes whose magnitude again shows a phase-locked state of equal-amplitude pulses. (b) Corresponding experimental spectrum (solid curve), fitted by the spectrum (open circles) of two 610-fs sech-profiled pulses, separated by 6.8 ps, and with a $-\pi/2$ phase difference. (c) Relative quadratic error between the experimental and the fitted curves versus the fitting phase. The minimum error is for a phase of $-91°$.

ity, between the optical isolator and the anomalous fiber. Although the overall shape of the spectra is slightly modified, the interfringe keeps the same value, with a measurement accuracy of 10^{-3}. This fact indicates that, although pulses are individually modified along their propagation in the cavity because of dispersion management, gain, losses, and nonlinearity, the bunch pattern is kept the same all along the cavity. We also changed the cavity average dispersion by reducing the length of the

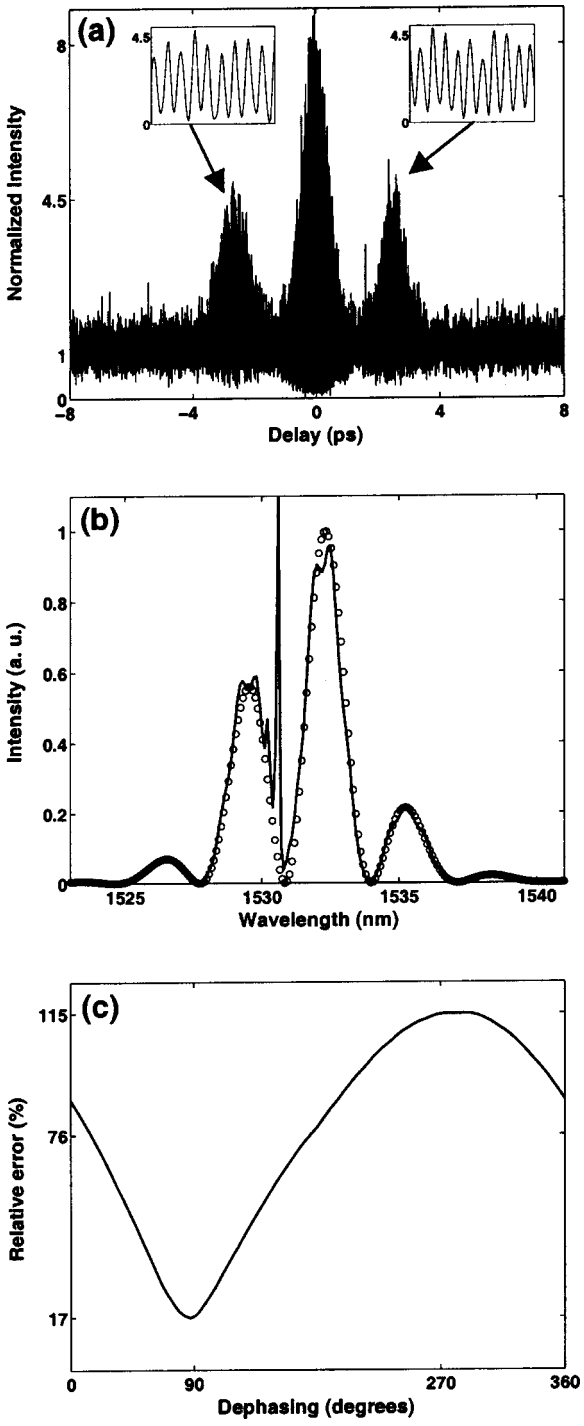

Fig. 6. Characteristics of a closer pulse pair. The pump power is 29 mW. (a) Interferometric autocorrelation that yields a 2.7-ps separation between phase-locked pulses of 540-fs duration. (b) Experimental spectrum (solid curve) fitted by the spectrum (open circles) of two 540-fs sech-profiled pulses separated by 2.7 ps and with a $\pi/2$ phase difference. (c) The plot of the relative fitting error versus the phase has a minimum for a phase of $+87°$.

anomalous fiber. Reaching the normal regime with an average dispersion of -5 (ps/nm)/km, we still observed the formation of phase-locked pulses with a separation of $\approx$20 ps. However in this regime that favors higher-energy and shorter single pulses,[28] multiple pulsing was more difficult to obtain and required a high pump power (300 mW). In our setup, the preferred pulse-to-pulse separation range is 19–23 ps; the next choice is 10–12 ps. In these cases, the large pulse-to-pulse separation (from 20 to 50 pulse widths) does not allow the spectra analysis to yield precise measurement of the phase difference between pulses. When the bunch comprises more than two pulses, closer separation ranges are difficult to stabilize, although we also observed several close pulse pairs equally separated as in Ref. 27.

3. PHASE-LOCKED PULSE PAIRS

In the anomalous average-dispersion regime, phase-locked pulse pairs are obtained at a moderate pump power that ranges, according to the mode-locking settings, from 60 to 100 mW and yields an output power that ranges from 0.5 to 2 mW. Mode-locking and pulse-bunching working points present large hysteresis with respect to the pump power. In particular, the phase-locked pulse pairs are conserved when the pump power is reduced to 40 mW. If the pump power were lowered further, the pulse pair would become, unstable and then lock again at a smaller separation. The same process can be repeated two or three times. Figures 5(a) and 6(a) show such close pulse pairs with separations of 6.8 and 2.7 ps, respectively. A tiny change in one of the mode-locking wave plates is often needed to stabilize the laser with a smaller separation. The jump behavior of the pulse separation seems related to the high degree of stability of the phase-locked pulse pairs. In particular, phase-locked states are immune to small alterations in pump power and wave plate settings. However, smaller separations, which are inherent in smaller intracavity powers, are less immune to perturbations than larger separations.

With a pair separation of less than 15 pulse widths, the phase relationship between the two phase-locked pulses can be inferred with good precision from the position of fringes in the pair spectrum. Figures 5(b) and 6(b) show strongly asymmetric spectra indicating that the phase relation between pulses is neither 0 nor π. The fitting procedure is as follows: from the autocorrelation trace, pulse width and separation are measured, then the only free parameter to fit the corresponding spectrum is the phase relationship of the pulse pair. The spectrum of Fig. 5(b) is well fitted by the spectrum that results from two 610-fs FWHM sech-profiled pulses separated by 6.8 ps and having a phase difference of $-\pi/2$. Figure 5(c) presents the mean quadratic error between the fit and the actual spectrum versus the phase whose optimum phase is $-91°$. The spectrum of Fig. 6(b) is fitted by the spectrum of two 540-fs sech-profiled pulses separated by 2.7 ps and having a $+\pi/2$ phase relationship.

It was the first time, to the best of our knowledge, that these $\pm\pi/2$ phase relationships were experimentally reported for a bound state of pulses.[16] In the literature, however, stable $\pm\pi/2$ phase-locked soliton pairs have been theoretically predicted within the framework of the complex Ginzburg–Landau equation.[15] Note that in passive optical fibers, in the absence of loss and gain, the interaction of two adjacent pulses does not usually lead to fixing the pulse-to-pulse separation: two solitons either attract or repel each other according to their phase relationship in such a way that no stable separation can be maintained. However, the addition of new source terms in the nonlinear Schrödinger equation (NSE) that was used to model propagation in the optical fiber could alter the latter statement.[31–33] In Refs. 32 and 33 the addition of loss, detuning, and pumping terms lead in some particular cases to the phase locking of solitons without imposing a systematic phase relationship (such as $\pi/2$) between paired solitons.

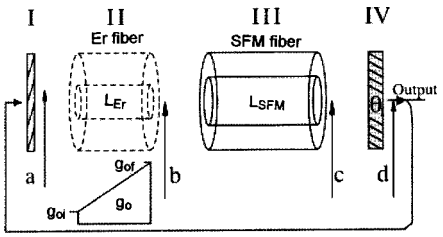

Fig. 7. Scheme of the theoretical model, which is thoroughly detailed in the main text.

To model real systems such as transmission lines and fiber lasers, additional terms such as linear and nonlinear gain, losses, and spectral filtering often need to be incorporated. The addition of these new terms could lead to the complex quintic Ginzburg–Landau equation (CQGLE).[34] The dynamics of a dissipative system described by the CQGLE is different from the dynamics of a conservative system described by the NSE. Solutions of the CQGLE result from a double balance, namely, between nonlinearity and dispersion and between gain and loss. In addition, the existence of more parameters in the CQGLE than in the NSE gives extra degrees of freedom to find stable multisoliton solutions, such as stable soliton pairs. The stability analysis of soliton pairs done in Ref. 15 showed that the phase difference between the two solitons converged to $\pm\pi/2$ as the soliton pair stabilized. Recently, an extension of this numerical work was performed to take into account propagation in dispersion-managed fiber links.[35] Periodic solutions with $\pm\pi/2$ phase-locked pairs as centers of oscillation were obtained.

Nevertheless, the CQGLE is a distributed equation model that cannot strictly apply to our fiber ring laser, since the pulses undergo strong changes in one cavity round trip. We then developed a more appropriate numerical model, as described in Section 4.

4. NUMERICAL SIMULATION OF PHASE LOCKING

The numerical model of our fiber laser ring cavity is presented in Fig. 7. It basically consists of four different parts that represent I, a wave-retarder plate characterized by its dephasing Δ and orientation θ_2 relative to the fast axis of the erbium fiber; II, the EDF; III, the anomalous single-mode fiber (SMF); IV, a polarizer whose axis forms a certain angle θ_1 with respect to the fast axis of

the birefringent SMF. For the sake of simplification, the two fibers share the same principal axes. Among other possible choices, the wave plate is chosen to be a quarter-wave plate, i.e., $\Delta = 90°$, oriented to transform the linearly polarized field after the polarizer into a circular state, namely, $\theta_1 - \theta_2 = 45°$. Between the different parts, at points a, b, c, and d, lumped linear losses are assumed to represent the real cavity losses that are due to splices, power rejection, and air-to-fiber coupling, which means there are 1-dB losses at points a, b, and c, and 2-dB losses at point d. The field is monitored after point d.

The field propagation in the EDF is governed by the following equations:

$$iU_z + \gamma' U + \frac{D}{2}U_{tt} + \Gamma|U^2|U + \frac{2}{3}\Gamma|V^2|U + \frac{1}{3}\Gamma V^2 U^* = ig(Q_U)U + i\beta U_{tt},$$

$$iV_z - \gamma' V + \frac{D}{2}V_{tt} + \Gamma|V^2|V + \frac{2}{3}\Gamma|U^2|V + \frac{1}{3}\Gamma U^2 V^* = ig(Q_V)V + i\beta V_{tt}, \quad (1)$$

where U and V are the normalized envelopes of the two polarization components of the optical field, γ' is the half-difference between the propagation constants of these two components, β is the strength of the spectral filtering, which is due mainly to the optical gain-limited bandwidth ($\beta > 0$). The other parameters are defined as follows:

$$D = \frac{\beta_2^{\mathrm{EDF}}}{\beta_2^{\mathrm{SMF}}}, \quad (2)$$

where β_2^{EDF} and β_2^{SMF} stand for the dispersion coefficients in the EDF and in the anomalous SMF, respectively,

$$\Gamma = \frac{A_{\mathrm{eff}}^{\mathrm{SMF}}}{A_{\mathrm{eff}}^{\mathrm{EDF}}}, \quad (3)$$

where $A_{\mathrm{eff}}^{\mathrm{SMF}}$ and $A_{\mathrm{eff}}^{\mathrm{EDF}}$ are the effective areas of each type of fiber.

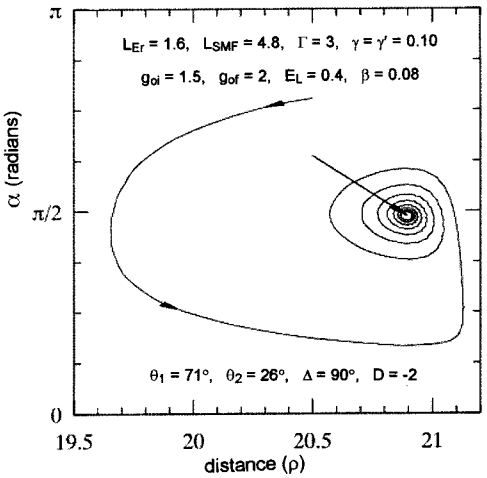

Fig. 8. Trajectory of the numerical simulation in the (ρ, α) plane of two interacting pulses: ρ represents the pulse-to-pulse separation, whereas α is their relative phase. The values for the parameters used in this simulation are listed in the figure.

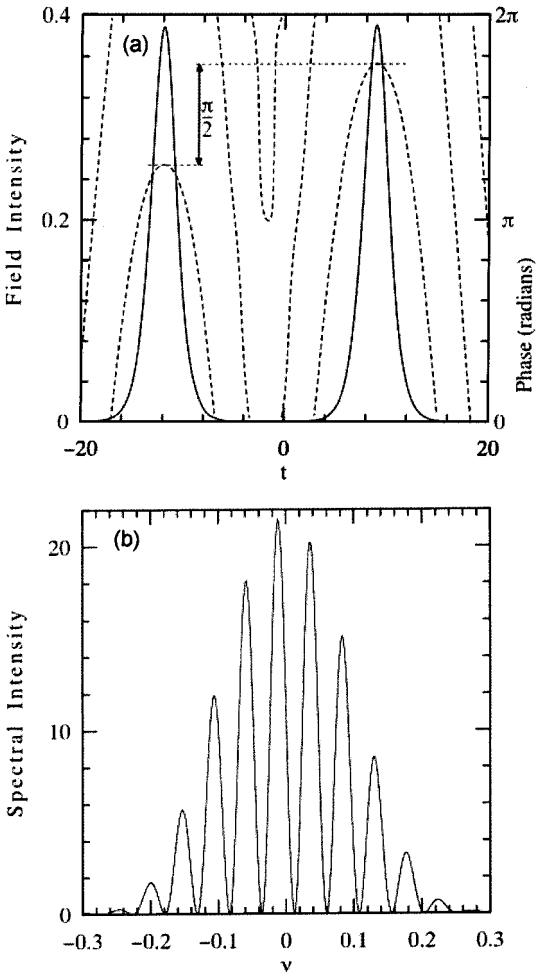

Fig. 9. (a) Intensity profile (solid curve) and phase profile (dotted curve) of one stationary solution. The time unit is 145 fs. (b) Corresponding optical spectrum. The parameters have the same value as in Fig. 7.

The function $g[Q_{U(V)}]$ represents the gain of the cavity that is due to an active medium having a recovery time much longer than the round-trip time of the cavity and therefore does not depend explicitly on time t. It can be modeled through

$$g[Q_{U(V)}] = \frac{g_0(z)}{1 + Q_{U(V)}/E_L}, \quad (4)$$

where E_L is the saturation energy and $Q_{U(V)}$ is the intracavity energy on the fast (slow) principal axis given by

$$Q_U = \int_{-\infty}^{+\infty} |U|^2 \mathrm{d}t, \qquad Q_V = \int_{-\infty}^{+\infty} |V|^2 \mathrm{d}t. \quad (5)$$

Here we used a model that accounts for polarization-dependent gain, an effect that could occur in high-power fiber amplifiers.[36,37] However, we checked numerically that taking the total intracavity energy Q instead of $Q_{U(V)}$, while doubling the saturation energy E_L and keeping the other parameters unaffected, obtained almost the same results. The small-signal gain is $g_0(z)$, which could depend on z to take into account pump depletion. For a first-order approximation, one can use

$$g_0(z) = g_{0i} + \frac{(g_{0f} - g_{0i})z}{L_{\mathrm{EDF}}}, \tag{6}$$

where g_{0i} and g_{0f} are the corresponding small-signal gains at both ends of the EDF of length L_{EDF}, as indicated in Fig. 7.

The pulse is then inserted into the SMF, and its evolution is governed by the following coupled-nonlinear equations[37]:

$$iU_z + \gamma U + \frac{1}{2}U_{tt} + |U|^2U + \frac{2}{3}|V|^2U + \frac{1}{3}V^2U^* = 0,$$

$$iV_z - \gamma V + \frac{1}{2}V_{tt} + |V|^2V + \frac{2}{3}|U|^2V + \frac{1}{3}U^2V^* = 0, \tag{7}$$

where γ is the half-difference between the propagation constants of the two field components. After the polarizer, the field becomes

$$U' = U\cos\theta_1 + V\sin\theta_1, \tag{8}$$

then passes through the wave plate, and the process repeats itself until some stationary solution is found. By taking any arbitrary input as the initial condition and by properly choosing the angle of polarizer θ_1 while keeping $\theta_1 - \theta_2 = 45°$ and fixing the rest of the cavity parameters, after many round trips we found a stationary solution. This stationary solution consists of one or several pulses, depending on the value of saturation energy E_L and small-signal gain g_0, because these two quantities are related to the amount of pump power used in the experiment.

The relation between the adimensional magnitudes z, t, U, V used above and the real magnitudes Z, T, E_x, E_y is as follows[13]:

$$z = \frac{Z}{Z_0}, \qquad Z_0 = \frac{T_0^2}{|\beta_2^{\mathrm{SMF}}|}, \qquad t = \frac{T - \frac{Z}{v_g}}{T_0},$$

$$\frac{U}{E_x} = \frac{V}{E_y} = \sqrt{\frac{RT_0{}^2}{|\beta_2^{\mathrm{SMF}}|}}, \qquad R = \frac{2\pi n_2}{\lambda A_{\mathrm{eff}}^{\mathrm{SMF}}}. \tag{9}$$

To run simulations of the experimental setup described in Section 2, we used the following values:

$$A_{\mathrm{eff}}^{\mathrm{SMF}} = 80\ \mu\mathrm{m}^2, \qquad A_{\mathrm{eff}}^{\mathrm{EDF}} = 27\ \mu\mathrm{m}^2,$$

$$n_2 = 2.5 \times 10^{-20}\ \mathrm{m}^2/\mathrm{W},$$

$$\beta_2^{\mathrm{SMF}} = -21\mathrm{ps}^2/\mathrm{km}, \qquad D = -2.$$

Let us add that there is no critical dependence of the numerical results on these numerical values. Taking $Z_0 = 1.00$ m fixes our time unit to be $T_0 = 145$ fs.

When two pulses appear, the evolution of their relative phase (α) and separation distance (ρ) converges to a fixed value, as shown in Fig. 8. A separate arrow points toward the stationary solution, which corresponds to a $\pi/2$ phase-locked state. Figures 9(a) and 9(b) detail the features of this stationary solution. In Fig. 9(a), both intensity and phase profiles are plotted, clearly showing two identical pulses with a $\pi/2$ phase difference. The FWHM of each pulse is around 3.0 units, which corresponds to $\approx$435 fs, whereas the distance between pulses is 21 units, which corresponds to 3.0 ps. The optical spectrum of this solution is shown in Fig. 9(b) and is in good agreement with the experimental spectra. The energy per pulse obtained in the simulation is $\approx$70 pJ, which is also similar to experimental values. The simulations presented here clearly demonstrate that soliton–soliton interactions in a dissipative system, such as a fiber laser, are responsible for the formation of stable phase-locked soliton pairs.

5. CONCLUSIONS

Phase-locked pulses were experimentally observed in a large variety of pulse-bunching configurations. These locked states, which form spontaneously, are stable and can remain for hours without active stabilization of the laser output. In the case of close pulse pairs, we could confirm by numerical simulation the $\pm\pi/2$ phase relationship obtained experimentally between the two pulses. The case of largely separated phase-locked pulses is much more difficult to simulate numerically because of the different time scales involved. We believe that large separations, which are the most common in our experiment, could imply a balance between phase-insensitive forces to fix an approximate separation. Mechanisms such as electrostriction and gain recovery could be involved. However, the existence of phase locking would indicate that the phase-sensitive soliton–soliton interactions described in Section 4 might act efficiently up to, and possibly at more than, 40 pulse widths.

The research of J. M. Soto-Crespo was supported under contract BFM2000-0806. Ph. Grelu's e-mail address is Philippe.Grelu@u-bourgogne.fr.

REFERENCES

1. D. J. Richardson, R. I. Laming, D. N. Payne, V. J. Matsas, and M. W. Phillips, "Pulse repetition rates in passive, self-starting, femtosecond soliton fibre laser," Electron. Lett. **27**, 1451–1453 (1991).
2. M. J. Guy, D. U. Noske, and J. R. Taylor, "Generation of femtosecond soliton pulses by passive mode locking of an ytterbium–erbium figure-of-eight fiber laser," Opt. Lett. **18**, 1447–1449 (1993).
3. M. Nakazawa, E. Yoshida, and Y. Kimura, "Low threshold, 290 fs erbium-doped fiber laser with a nonlinear amplifying loop mirror pumped by InGaAsP laser diodes," Appl. Phys. Lett. **59**, 2073–2075 (1991).
4. A. B. Grudinin, D. J. Richardson, and D. N. Payne, "Energy quantisation in figure eight fibre laser," Electron. Lett. **28**, 67–68 (1992).
5. T. Tsang, "Observation of high-order solitons from a mode-locked Ti:sapphire laser," Opt. Lett. **18**, 293–295 (1993).
6. Ch. Spielmann, P. F. Curley, T. Brabec, and F. Krausz, "Ultrabroadband femtosecond lasers," IEEE J. Quantum Electron. **30**, 1100–1114 (1994).
7. M. Lai, J. Nicholson, and W. Rudolph, "Multiple pulse operation of a femtosecond Ti:sapphire laser," Opt. Commun. **142**, 45–49 (1997).
8. B. Chassagne, G. Jonusauskas, J. Oberlé, and C. Rullière, "Multipulse operation regime in a self-mode-locked Cr^{4+}: forsterite femtosecond laser," Opt. Commun. **150**, 355–362 (1998).

9. J. P. Gordon, "Dispersive perturbations of solitons of the nonlinear Schroedinger equation," J. Opt. Soc. Am. B **9**, 91–97 (1992).
10. S. M. J. Kelly, "Characteristic sideband instability of periodically amplified average soliton," Electron. Lett. **28**, 806–807 (1992).
11. J. Herrmann, V. P. Kalosha, and M. Müller, "Higher-order phase dispersion in femtosecond Kerr-lens mode-locked solid-state lasers: sideband generation and pulse splitting," Opt. Lett. **22**, 236–238 (1997).
12. F. Gutty, Ph. Grelu, N. Huot, G. Vienne, and G. Millot, "Stabilisation of modelocking in fibre laser through pulse bunching," Electron. Lett. **37**, 745–746 (2001).
13. G. P. Agrawal, *Nonlinear Fiber Optics*, 2nd ed. (Academic, San Diego, Calif., 1995).
14. B. A. Malomed, "Bound solitons in the nonlinear Schrödinger–Ginzburg–Landau equation," Phys. Rev. A **44**, 6954–6957 (1991).
15. N. N. Akhmediev, A. Ankiewicz, and J. M. Soto-Crespo, "Stable soliton pairs in optical transmission lines and fiber lasers," J. Opt. Soc. Am. B **15**, 515–523 (1998).
16. Ph. Grelu, F. Belhache, F. Gutty, and J. M. Soto-Crespo, "Phase-locked soliton pairs in a stretched-pulse fiber laser," Opt. Lett. **27**, 966–968 (2002).
17. A. B. Grudinin, D. J. Richardson, and D. N. Payne, "Passive harmonic mode-locking of a fibre soliton ring laser," Electron. Lett. **29**, 1860–1861 (1993).
18. A. B. Grudinin and S. Gray, "Passive harmonic mode locking in soliton fiber lasers," J. Opt. Soc. Am. B **14**, 144–154 (1997).
19. K. Tamura and M. Nakazawa, "Dispersion-tuned harmonically mode-locked fiber ring laser for self-synchronization to an external clock," Opt. Lett. **21**, 1984–1986 (1996).
20. T. F. Carruthers, I. N. Duling III, M. Horowitz, and C. R. Menyuk, "Dispersion management in a harmonically mode-locked fiber soliton laser," Opt. Lett. **25**, 153–155 (2000).
21. K. S. Abedin, N. Onodera, and M. Hyodo, "Generation of a 64-GHz, 3.3-ps transform-limited pulse train from a fiber laser employing higher-order frequency-modulated mode locking," Opt. Lett. **24**, 1564–1566 (1999).
22. C. X. Yu, H. A. Haus, E. P. Ippen, W. S. Wong, and A. Sysoliatin, "Gigahertz-repetition-rate mode-locked fiber laser for continuum generation," Opt. Lett. **25**, 1418–1420 (2000).
23. N. H. Bonadeo, W. H. Knox, J. M. Roth, and K. Bergman, "Passive harmonic mode-locked soliton fiber laser stabilized by an optically pumped saturable Bragg reflector," Opt. Lett. **25**, 1421–1423 (2000).
24. N. H. Seong, D. Y. Kim, and S. K. Oh, "Self-adjustments of positions of quantised modelocked pulses in figure-eight fibre laser," Electron. Lett. **37**, 157–158 (2001).
25. A. N. Pilipetskii, E. A. Golovchenko, and C. R. Menyuk, "Acousic effect in passively mode-locked fiber ring lasers," Opt. Lett. **20**, 907–909 (1995).
26. J. N. Kutz, B. C. Collings, K. Bergman, and W. H. Knox, "Stabilized pulse spacing in soliton lasers due to gain depletion and recovery," IEEE J. Quantum Electron. **34**, 1749–1757 (1998).
27. D. Y. Tang, W. S. Man, H. Y. Tam, and P. D. Drummond, "Observation of bound states of solitons in a passively mode-locked fiber laser," Phys. Rev. A **64**, 33814 (2001).
28. K. Tamura, L. E. Nelson, H. A. Haus, and E. P. Ippen, "Soliton versus nonsoliton operation of fiber ring lasers," Appl. Phys. Lett. **64**, 149–151 (1994).
29. K. Tamura, E. P. Ippen, and H. A. Haus, "Pulse dynamics in stretched-pulse fiber lasers," Appl. Phys. Lett. **67**, 158–160 (1995).
30. V. J. Matsas, T. P. Newson, D. J. Richardson, and D. N. Payne, "Self-starting passively mode-locked fibre ring soliton laser exploiting nonlinear polarisation rotation," Electron. Lett. **28**, 1391–1393 (1991).
31. N. N. Akhmediev and S. Wabnitz, "Phase detecting of solitons by mixing with a continuous-wave background in an optical fiber," J. Opt. Soc. Am. B **9**, 236–242 (1992).
32. S. Wabnitz, "Suppression of interactions in a phase-locked soliton optical memory," Opt. Lett. **18**, 601–603 (1993).
33. S. Wabnitz, "Control of soliton train transmission, storage, and clock recovery by cw light injection," J. Opt. Soc. Am. B **13**, 2739–2749 (1996).
34. J. D. Moores, "On the Ginzburg–Landau laser mode-locking model with fifth-order saturable absorption terms," Opt. Commun. **96**, 65–70 (1993).
35. N. Akhmediev, F. Zen, and P. Chu, "Pulse–pulse interaction in dispersion-managed fiber systems with nonlinear amplifiers," Opt. Commun. **201**, 217–221 (2002).
36. P. C. Becker, N. A. Olsson, and J. R. Simpson, *Erbium-Doped Fiber Amplifiers, Fundamentals and Technology* (Academic, San Diego, Calif., 1999).
37. J. M. Soto-Crespo, N. N. Akhmediev, B. C. Collings, S. T. Cundiff, K. Bergman, and W. H. Knox, "Polarization-locked temporal vector solitons in a fiber laser: theory," J. Opt. Soc. Am. B **17**, 366–372 (2000).